Supporting Information:

Flexible random lasers with tunable lasing emissions

Ya-Ju Lee, [*a] Chun-Yang Chou, [a] Zu-Po Yang, [*b] Nguyen Thi Bich Hanh, [a] Yung-Chi Yao, [a] Ting-Wei Yeh, [a] Meng-Tsan Tsai, [*cd] and Hao-Chun Kuo [e]

[a] Institute of Electro-Optical Science and Technology, National Taiwan Normal University, 88, Sec.4, Ting-Chou Road, Taipei 116, Taiwan; Fax: +886-2-86631954; Tel: +886-2-77346733; E-mail: yajulee@ntnu.edu.tw

[b] Institute of Photonic System, National Chiao-Tung University, 301, Gaofa 3rd Road, Tainan 711, Taiwan; E-mail: zupoyang@nctu.edu.tw

[c] Department of Electrical Engineering, Chang Gung University, 259, Wenhua 1st Rd., Taoyuan, 33302, Taiwan; E-mail: mttsai@mail.cgu.edu.tw

[d] Department of Dermatology, Chang Gung Memorial Hospital, Linkou, Taiwan

[e] Department of Photonics and Institute of Electro-Optical Engineering, National Chiao Tung University, Hsinchu, 300, Taiwan

Evolution of the absorption spectrum of Ag NPRs with different synthesis times

Figure S1 shows the evolution of the absorption spectrum of Ag NPRs when the synthesis time was increased from 2 to 10 minutes. As mentioned in the experimental section of the article, the addition of $NaBH_4$ into the mixed aqueous solution ($AgNO_3/Na_3C_6H_5O_7/C_2H_6O/H_2O_2$) induces the reduction of silver. This instantly changes the solution color from the original colorless to light yellow and then to deep yellow within ~30 seconds. This indicates the formation of Ag nanoparticles. After that, the morphology of Ag particles started to vary and eventually evolved into nanoprism-shaped particles over the next few minutes (2–10 min), accompanied with the further change in solution color from deep yellow to red, purple, and blue (inset, Fig. S1). It should be noted that in this step, we continuously added proper amounts of $NaBH_4$ and stirred incessantly to ensure that the reaction of silver reduction is complete throughout the entire solution. According to Fig. S1, the original intensity of the absorption peak at ~408 nm associated with small Ag nanoparticles decreased considerably with the increase in the synthesis time, because of the consumption of small Ag nanoparticles during the reaction. Furthermore, a clear red shift was observed on another dominant absorption peak with an initial peak wavelength of ~514 nm, implying the dimension growth and well formation of Ag NPRs with the increase in synthesis time. In this study, we chose Ag NPRs with a synthesis time in between 3 and 6 min as the resultant LSP peak exhibited high spectral overlapping with the PL spectrum of R6G gain medium.

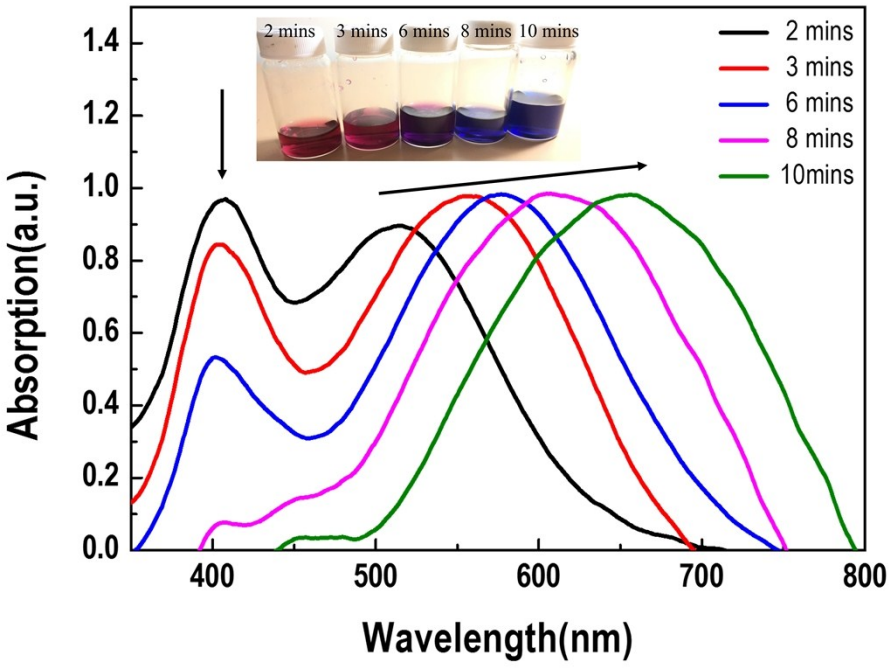

Figure S1. Evolution of the absorption spectrum of the Ag NPRs for the synthesis time from 2 to 10 min. Inset: photograph of a series of Ag NPR solutions with different synthesis times.

Emission of R6G in methanol for different dye concentrations

Figure S2 shows the normalized PL spectra of R6G dye dissolved in methanol with various R6G concentrations ranging from 10^{-2} to 10^{-6} g/ml. Accordingly, the peak wavelength of PL spectrum (λ_P) is red-shifted with the increase in R6G dye concentration. The R6G with the highest concentration solution (i.e., 10^{-2} g/ml) emits at λ_P = 562.2 nm. Dilution of concentration by addition of methanol leads to an obvious blue shift in λ_P. For the lowest R6G concentration of 10^{-6} g/ml, λ_P was at around 550.0 nm, moving away from the LSP peak of the Ag NPRs. λ_P does not shift to the longer wavelength range but remains constant at around 562.2 nm when we further increase the R6G concentration to 10^{-1} g/ml. Because such high concentration of R6G will cause non-uniformity in the spin coating on the PET substrate, we selected a R6G concentration of 10^{-2} g/ml as the treatment condition for the subsequent experiments in this study.

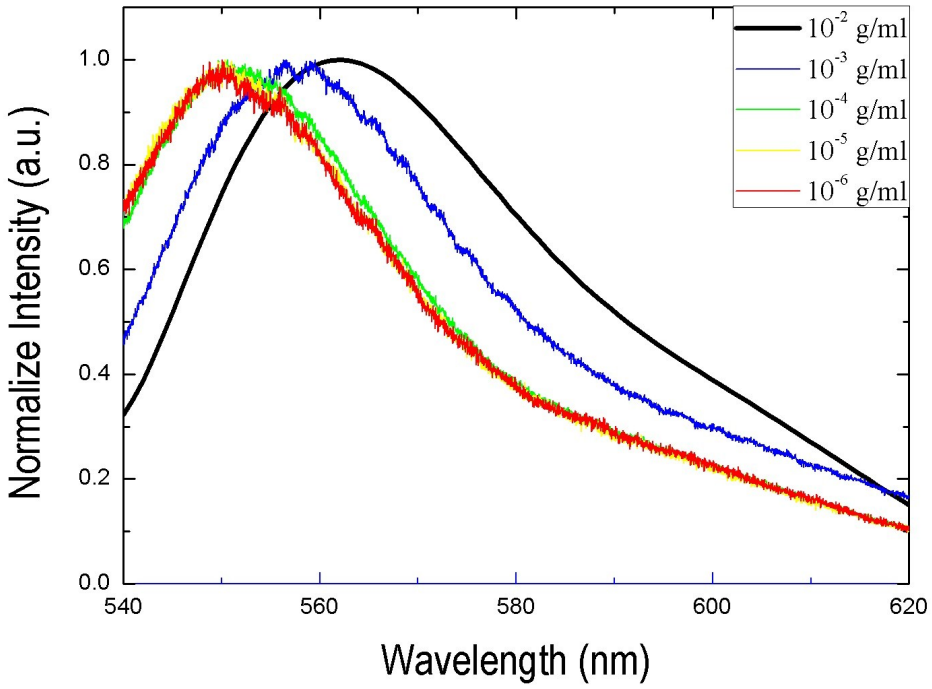

Figure S2. Normalized PL spectra of R6G dye dissolved in methanol with various R6G concentrations ranging from 10^{-2} to 10^{-6} g/ml.

Estimation of the spectral overlap between the R6G emission and Ag NPRs absorption

Figure S3 shows the overlapping spectra of the PL emission of R6G with the absorption spectrum of the Ag NPRs. In the present work, we purposely used a high concentration of R6G, i.e., 10^{-2} g/ml; therefore, λ_P of the PL emission of R6G was substantially red-shifted to 562.2 nm, and there was a significant spectral overlap between the absorption of Ag NPRs (blue line) and the PL emission spectrum of the R6G (red line). The number of Ag NPRs per milliliter of the solution was calculated by using the equation $N = (N_0C/1000f)(r/R)^3$, where N_0 is the Avogadro number (~6.02×10^{23}), C is the concentration of the silver precursor (0.01 mM), f is the packing fraction of the atoms (f = 0.74), r is the radius of silver atoms (r =1.22 Å), and R is the average radii of the Ag NPRs. Consequently, the number of Ag NPRs was estimated to be 9.46×10^{13} mL^{-1}, and the corresponding overlap integral according to Eq. (1) was thus estimated to be $J(\lambda) = 6.50 \times 10^{20}$ nm^4 M^{-1} cm^{-1}.

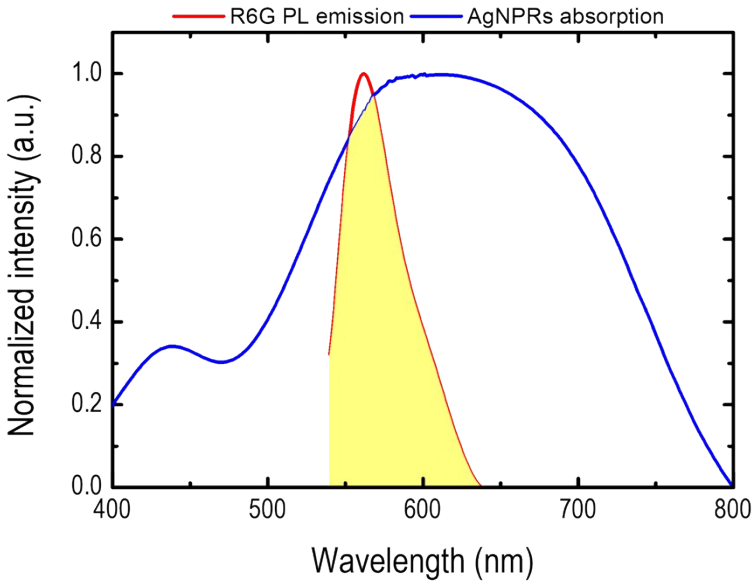

Figure S3. Overlap spectra of the PL emission of R6G with the absorption spectrum of the Ag NPRs.

Homemade tool for exerting bending strain on the PET substrate

Figure S4 shows the homemade tool, which can deform the PET substrate into a convex shape with a specific curvature. The distance between the two parallel acrylic sheets can be controlled by screwing the gears in the center. Thus, the bending diameter of the PET was tunable, which in turn varied the bending strain exerted on it.

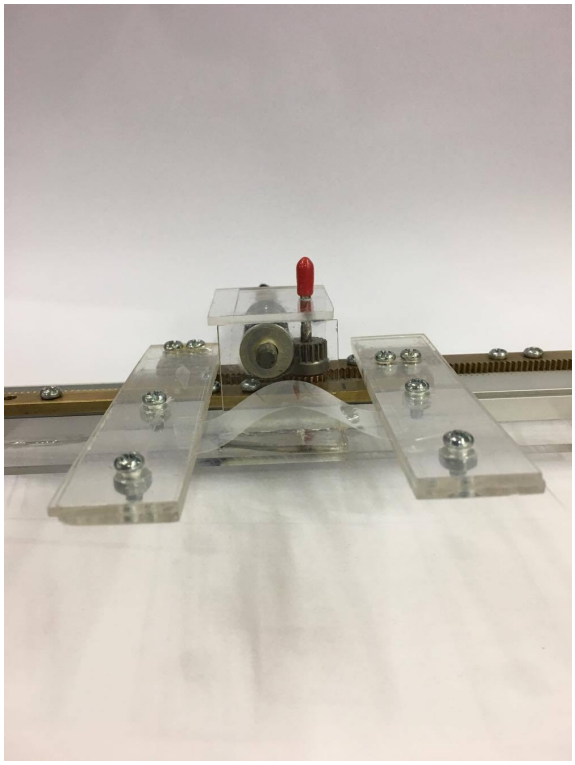

Figure S4. Homemade tool to control the bending strain exerted on the PET substrate.

Schematic configuration of FDTD simulation

Figure S5 shows the schematic for the calculation of the scattering spectrum of the Ag NPRs by using the FDTD simulation (OptiFDTD). For simplicity, the shape of Ag NPRs was set as an equilateral triangle, with an edge length of a = 90 nm and a thickness of h = 50 nm. The unit cell composed of such Ag NPRs is deployed on the y-z plane and arranged in the form of a hexagonal close-packed structure, and the interparticle distance between each Ag NPR is represented as d, which ranges from 100 to 300 nm, with 50-nm intervals. This develops a simulation scenario to reflect the distributed variation in the Ag NPRs when different bending strains were exerted on the PET substrate. We assumed that the interparticle distance between each Ag NPR increases monotonously with the increase in bending strains exerted on the PET substrate. A light wave of rectangular function (λ = 400–700 nm) with a linear polarization (parallel to the y-axis) propagating along the negative x-direction was incident on the Ag NPRs to excite the LPS resonance. This was accompanied by the light scattering in random directions. An observation surface was placed right above the Ag NPRs, and in between them, an opaque object with a slightly smaller blocking area than the observation surface was inserted to block the retro-reflection (or scattering light in the normal direction) by the Ag NPRs. From this configuration of FDTD simulation, the observation surface could mainly detect the scattering light, which was scattered by the Ag NPRs to be inclined in the lateral directions, which is close to our experimental condition for measuring the scattering spectrum by the dark-field microscopy.

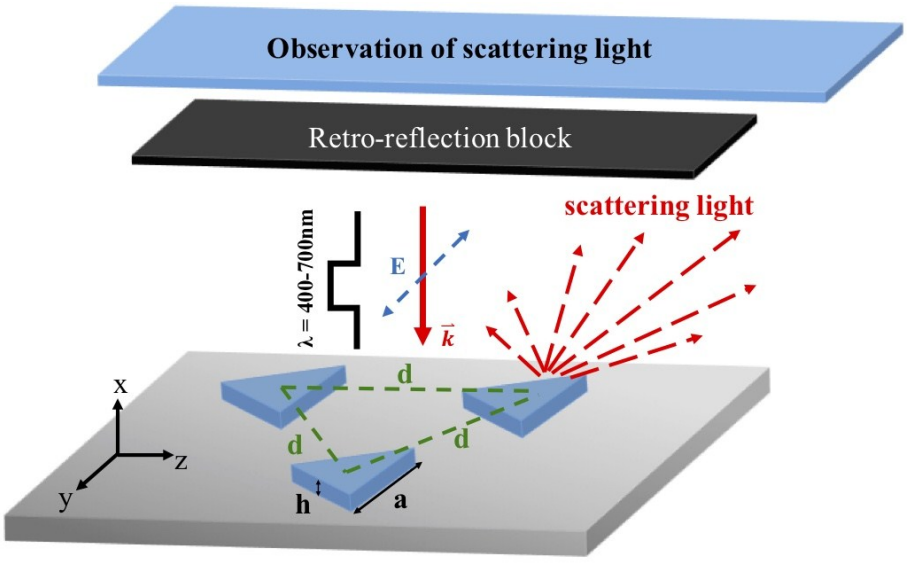

Figure S5. Schematic illustration of physical parameters and coordinate system adopted in the FDTD simulation.

FDTD simulations of electric field distribution in the Ag NPRs

Figure S6 shows the FDTD simulations of the electric field profile (Ey) for the Ag NPRs with d =100 nm (left panel) and d = 300 nm (middle panel) at λ = 600 nm. The simulated Ey profile of single Ag NPR (i.e., equivalent to the case that d is infinity) is plotted in the right panel of Fig. S6. For a given optical wavelength, the mutual coupling of surface plasmons between Ag NPRs strongly depends on the interparticle distance d, which in turn affects the scattering degree of the emitted photons. When d was increased, the mutual coupling of surface plasmon between Ag NPRs became weak and tended to disappear, thus altering the scattering ability for the different emitted photon energies. However, the FDTD simulation is only an initial step that provides a qualitative illustration and one possible mechanism for the blue shift in the measured scattering spectrum. Further experiments are necessary before we can conclude the physical rationale for the observed effect.

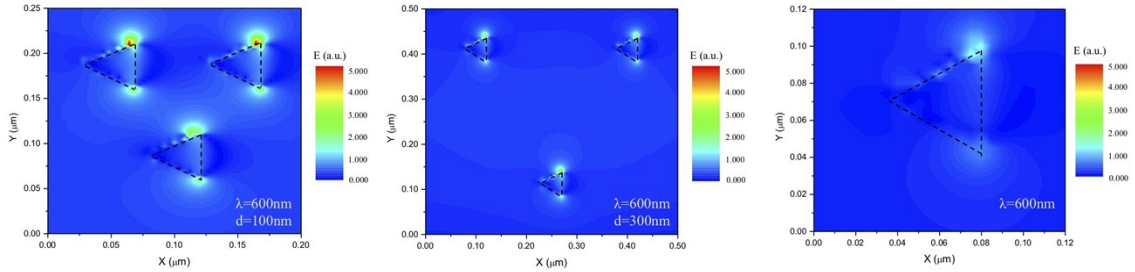

Figure S6. FDTD simulations of the electric field distribution (Ey) for the Ag NPRs with d =100 nm (left panel) and d = 300 nm (middle panel) at λ = 600 nm. Simulated Ey profile of single Ag NPR is plotted in the right panel of the figure.

FDTD-simulated scattering spectra of the Ag NPRs with different edge lengths

Figure S7 shows the FDTD-simulated scattering spectra of the Ag NPRs with different edge lengths ranging from 50 to 70 nm, with a 5-nm interval, whereas the interparticle distance d was kept constant at 300 nm. Accordingly, the position of the spectral maximum of the scattering spectrum strongly depended on the dimension of the Ag NPRs, and this might be one of the possible reasons responsible for the observed oscillation phenomenon in the measured scattering spectra as a dimension variation existed in the Ag NPRs during their synthesis process.

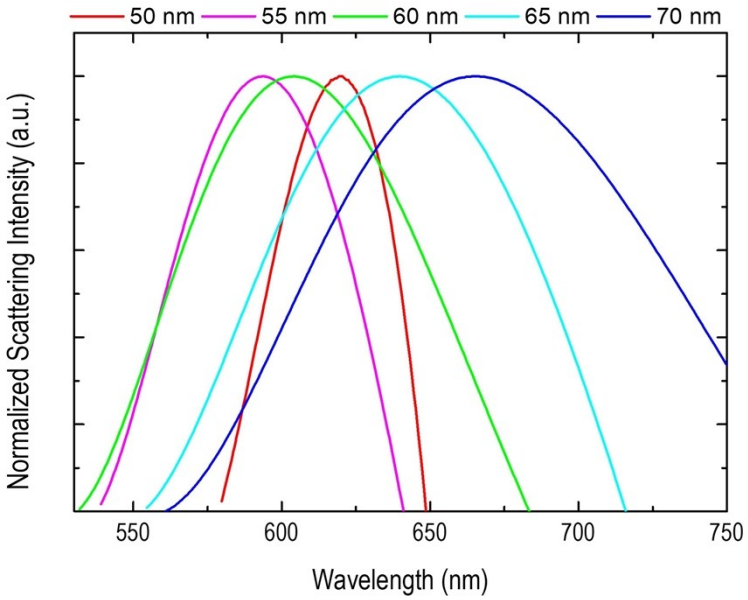

Figure S7. FDTD-simulated scattering spectra of the Ag NPRs with different edge lengths ranging from 50 to 70 nm, with an interval of 5 nm.

Reporting checklist for manuscript with a claim of lasing

To confirm if our observations are according to lasing behavior, we follow the check list of Nature "Reporting checklist for manuscripts with a claim of lasing" point by point as follows:

1. Peak intensities of the emission spectrum of our devices versus pump power were plotted over a wide range of values (20-70 μJ), as shown in Fig. 4(b) of the manuscript. Accordingly, the corresponding slope rises clearly and rapidly above a certain threshold in pump power.
2. As shown in Fig. 4(a) of the manuscript, we plotted the variation in spectral emission at pump powers below, around, and above the threshold. We observed a clear linewidth narrowing of the spectral emission at the lasing transition. The resolution of the spectrometer used in this study was 0.25 nm.
3. The spatial profile of the lasing emission was obtained as shown in the image of the cover letter, and our random laser indicates the existence of a well-defined stripe beam above the threshold (The incident pump laser was focused on the central area of the fabricated device in a strip shape of 50-μm width and 6.0-mm length by a cylindrical lens at an incidence angle of 45° with respect to the surface normal).
4. In this study, we used a frequency-doubled Q-switched Nd:YAG laser as the pump source with a pulse duration of 5 ns, wavelength of 532 nm, and repetition rate of 10 Hz. The incident pump laser was focused on the central area of the fabricated device in a strip shape of 50-μm width and 6.0-mm length by a cylindrical lens. Therefore, the thresholds of fabricated devices ranged from 0.0128 to 0.0158 J cm^{-2}.
5. We ruled out the other explanations such as amplified spontaneous emission, directional scattering, and modification of fluorescence spectrum by the cavity (in fact, there is was regular cavity in the random laser) as being responsible for the emission properties of our devices. We confirmed that the observed emission characteristics of the fabricated devices are attributed to the stimulated emission.
6. We fabricated three devices for each structure, i.e., the R6G film decorated with and without the Ag NPRs, and each device was tested for several times. As shown in Fig. 7 of the manuscript, we also conducted a mechanical durability test to repetitively bend the fabricated devices (30 times/min) and to examine their stability. Accordingly, the threshold of pump power required to stimulate random lasing emissions of the fabricated device barely changed, even after the 1000-time bending test, suggesting that the fabricated devices are reliable, and the corresponding measured characteristics are stable.

In accordance with the information provided above, we therefore confirmed and made a claim of the lasing action in the device fabricated in the present study.